SCIENTIFIC REPORTS

OPEN

SUBJECT AREAS:
QUANTUM METROLOGY
ULTRACOLD GASES

Received
26 July 2013

Accepted
22 October 2013

Published
7 November 2013

Correspondence and requests for materials should be addressed to G.C. (chengang971@163.com)

Orbit-induced spin squeezing in a spin-orbit coupled Bose-Einstein condensate

Jinling Lian[1,2], Lixian Yu[1,3], J.-Q. Liang[2], Gang Chen[1] & Suotang Jia[1]

[1]State Key Laboratory of Quantum Optics and Quantum Optics Devices, Institute of Laser spectroscopy, Shanxi University, Taiyuan 030006, P. R. China, [2]Institute of Theoretical Physics, Shanxi University, Taiyuan 030006, P. R. China, [3]Department of Physics, Shaoxing University, Shaoxing 312000, P. R. China.

In recent pioneer experiment, a strong spin-orbit coupling, with equal Rashba and Dresselhaus strengths, has been created in a trapped Bose-Einstein condensate. Moreover, many exotic superfluid phenomena induced by this strong spin-orbit coupling have been predicted. In this report, we show that this novel spin-orbit coupling has important applications in quantum metrology, such as spin squeezing. We first demonstrate that an effective spin-spin interaction, which is the heart for producing spin squeezing, can be generated by controlling the orbital degree of freedom (i.e., the momentum) of the ultracold atoms. Compared with previous schemes, this realized spin-spin interaction has advantages of no dissipation, high tunability, and strong coupling. More importantly, a giant squeezing factor (lower than −30 dB) can be achieved by tuning a pair of Raman lasers in current experimental setup. Finally, we find numerically that the phase factor of the prepared initial state affects dramatically on spin squeezing.

The spin-orbit coupling (SOC) describes an intrinsic interaction between the spin and orbital degrees of freedom of a particle. In condensed-matter physics, the SOC of electron not only generates some important quantum phenomena such as the spin and anomalous Hall effects[1,2], and the topological insulators and topological superconductors[3], but also plays a key role in realizing the spintronics[4] and the topological quantum computing[5]. However, the observations of SOC physics in naturally-occurring solid-state systems are often hindered by the unavoidable disorder and impurity effects. In this context, the neutral atom gases provide an ideal platform for exploring novel SOC physics and device applications[6], owing to their unprecedented level of control and precision in experiments. Recently, a synthetic SOC, with equal Rashba and Dresselhaus strengths, has been created in a trapped Bose-Einstein condensate (BEC) by a pair of Raman lasers[7]. Moreover, its strength is far larger than that in the typical solid-state materials. Under the strong SOC strength, rich superfluid phenomena have been revealed[8–36]. Here we present that this novel SOC technique has important applications in quantum metrology, such as spin squeezing.

Spin squeezing is a quantum correlation with reduced fluctuations in one of the collective spin components[37]. It not only has possible applications in atom interferometers and high-precision atom clocks[38], but also is closely related to and implies quantum entanglement[39]. Nonlinear spin-spin interactions are the heart for producing spin squeezing[40]. In experiments, the multi-component BEC is a powerful system to achieve spin squeezing[41–49], since the required spin-spin interactions can be induced by the intrinsic atom-atom collision interactions. Although these atom-atom collision interactions can, in principle, be tuned widely by varying the scattering lengths via Feshbach resonances[50], the experimental achievements are still difficult, and thus the maximal squeezing factors measured experimentally are higher than −15 dB[51]. Moreover, the atom-atom collision interactions usually induce atom decoherence and dissipations, which limits the achievable squeezing factor[52,53].

In this report, we show that the important spin-spin interaction can be induced by controlling the orbital degree of freedom (i.e., the momentum) of the ultracold atoms in the trapped BEC, with the equal Rashba and Dresselhaus SOCs. Since the generated interaction by the orbit is an indirect spin-spin interaction, it has advantages of no dissipation, high tunability, and strong coupling, compared with previous schemes[41–49]. Then, we obtain an analytical spin squeezing factor by means of the frozen-spin approximation. Interestingly, the maximal squeezing factor can reach a large negative value (lower than −30 dB) by tuning the Raman lasers in current experimental setup of NIST. This giant squeezing factor is far larger than previous ones[51]. Finally, we find numerically that the phase factor of the prepared initial state affects dramatically on spin squeezing.

Results

Model and hamiltonian. Figure 1(a) shows the experimental setup of NIST for realizing the equal Rashba and Dresselhaus SOCs in the trapped BEC, with ^{87}Rb atoms[7]. In their experiment, all ultracold atoms are prepared in the xy plane, using a strong confinement along the z direction. Moreover, two hyperfine ground states, $|F = 1, m_F = -1\rangle$ and $|F = 1, m_F = 0\rangle$, act respectively as effective spin-↑ and spin-↓ components in a large detuning Δ from the excited state, as shown in Fig. 1(b). When these components are coupled by a pair of Raman lasers incident at a $\pi/4$ angle from the x axis, as shown in Fig. 1(a), the equal Rashba and Dresselhaus SOCs can be created in a dressed-state basis $\left(|\tilde{\uparrow}\rangle = \exp(i\mathbf{k}_1\cdot\mathbf{r})|\uparrow\rangle \text{ and } |\tilde{\downarrow}\rangle = \exp(i\mathbf{k}_2\cdot\mathbf{r})|\downarrow\rangle\right)$, where $\mathbf{k}_1$ and $\mathbf{k}_2$ are the wave vectors of the Raman lasers). The corresponding dynamics is governed by the following Gross-Pitaevskii (GP) equation[7]

$$i\hbar\frac{\partial\Phi}{\partial t} = \left(\frac{p^2}{2m} + V(\mathbf{r}) + H_{\rm SOC} + H_{\rm INT}\right)\Phi, \qquad (1)$$

where $\Phi = (\Phi_\uparrow, \Phi_\downarrow)^T$ is the normalization wave function in the dress-state representation. The harmonic trap potential $V(\mathbf{r}) = \frac{1}{2}m\left(\omega_x^2x^2 + \omega_y^2y^2\right)$, where m is the mass of the ultracold atom, and ω_x and ω_y are the trap frequencies in the x and y directions. The Hamiltonian for the equal Rashba and Dresselhaus SOCs is written as $H_{\rm SOC} = \gamma p_x\sigma_z + \hbar\Omega\sigma_x/2$, where $\gamma = \hbar k_L/m = \hbar\sqrt{2}\pi/(m\lambda)$ is the strength of SOC, λ is the wavelength of the Raman lasers, $\Omega = \Omega_1\Omega_2^*/2\Delta$ is an effective Rabi frequency, Ω_1 and Ω_2 are the Rabi frequencies of the Raman lasers, and σ_z and σ_x are the Pauli matrices. The mean-field atom-atom collision interactions $H_{\rm INT} = {\rm diag}(g_{\uparrow\uparrow}|\Phi_\uparrow|^2 + g_{\uparrow\downarrow}|\Phi_\downarrow|^2, g_{\uparrow\downarrow}|\Phi_\uparrow|^2 + g_{\downarrow\downarrow}|\Phi_\downarrow|^2)$, where $g_{\uparrow\uparrow} = g_{\uparrow\downarrow} = 4\pi\hbar^2N(c_0 + c_2)/(ma_z)$ and $g_{\downarrow\downarrow} = 4\pi\hbar^2Nc_0/(ma_z)$ reflect the inter- and intra- spin collision interactions, respectively, c_0 and c_2 are the s-wave scattering lengths, and $a_z = \sqrt{2\pi\hbar/m\omega_z}$ with trap frequency ω_z in the z direction.

Since the s-wave scattering lengths have been measured experimentally as $c_0 = 100.86\ a_B$ and $c_2 = -0.46\ a_B$[7], where a_B is the Bohr radius, we can find immediately that $g_{\uparrow\uparrow} = g_{\uparrow\downarrow} \simeq g_{\downarrow\downarrow}$. This means that the trapped BEC exhibits strong atom-atom collision interactions, which can force all ultracold atoms to occupy the same many-body quantum state. As a result, we can introduce two boson operators, $a = \sqrt{m\omega_x/2\hbar}(x + ip_x/m\omega_x)$ and $b = \sqrt{m\omega_y/2\hbar}(y + ip_y/m\omega_y)$, to map the Hamiltonian for the GP equation (1) into a generalized Dicke model $H_{\rm T} = \hbar\omega_yNb^\dagger b + \hbar\omega_xNa^\dagger a + \hbar\Omega S_x + \sqrt{2}\gamma\sqrt{m\hbar\omega_x}i(a^\dagger - a)S_z + \nu S_z^2$[21], where $S_z = N\sigma_z/2 = \left(\psi_\uparrow^\dagger\psi_\uparrow - \psi_\downarrow^\dagger\psi_\downarrow\right)/2$ and $S_x = N\sigma_x/2 = \left(\psi_\uparrow^\dagger\psi_\downarrow + \psi_\downarrow^\dagger\psi_\uparrow\right)/2$ are the collective spin operators, with the field operators $\psi_\uparrow$ and $\psi_\downarrow$ for the different spin components, and $\nu = (g_{\uparrow\uparrow} + g_{\downarrow\downarrow} - 2g_{\uparrow\downarrow})/4$ is an effective spin-spin interaction induced by the direct atom-atom collision interactions. Due to the fact $g_{\uparrow\uparrow} = g_{\uparrow\downarrow} \simeq g_{\downarrow\downarrow}$, this effective spin-spin interaction disappears ($\nu = 0$), but the strong atom-atom collision interactions have still remained. On the other hand, the boson mode in the y direction does not interact with the ultracold atoms. Thus, the system's properties of the spin-orbit coupled BEC in Fig. 1(a) is governed by the standard Dicke model[54]

$$H = \hbar\omega_xNa^\dagger a + \hbar\Omega S_x + \sqrt{2}\gamma\sqrt{m\hbar\omega_x}i(a^\dagger - a)S_z. \qquad (2)$$

We emphasize that the Hamiltonian (2) is valid for current experimental conditions of NIST. For a sufficiently strong repulsive interaction between the different spin components, i.e., $g_{\uparrow\downarrow} > 0$ and $g_{\uparrow\downarrow} \gg \{g_{\uparrow\uparrow}, g_{\downarrow\downarrow}\}$, the trapped BEC undergoes an imaginary excitation and is thus unstable[20,55]. In such a case, the mapping of the Dicke model is invalid. On the other hand, for the opposite limit that the trapped BEC has no interactions, including both the same and different spin components, all ultracold atoms occupy both $\pm K_{\rm min}\left(=\sqrt{\gamma^2 - \Omega^2/4\gamma^2}\right)$ in the momentum space with an artificial ratio[21], and there is no correlation between the ultracold atoms. This means that the resulting spatial distribution of the trapped BEC is artificial and the above single spatial mode approximation in the Hamiltonian (2) cannot be applied.

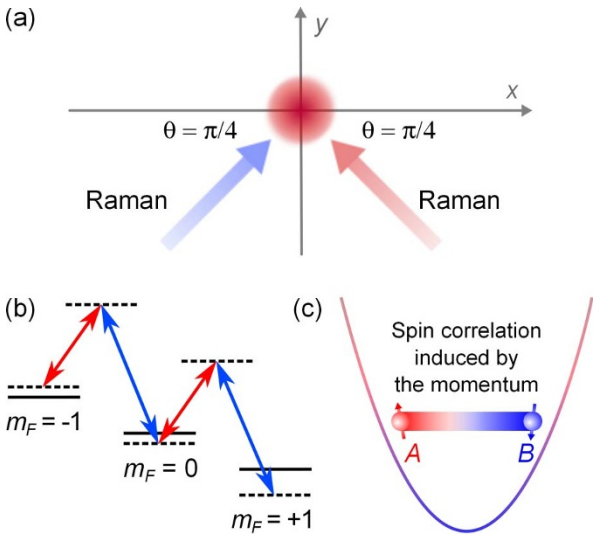

Figure 1 | Illustration about how to achieve spin squeezing, using the experimental setup of NIST. (a) The specified experimental setup for realizing the equal Rashba and Dresselhaus SOCs in the trapped BEC. (b) The energy levels, labeled respectively by $|F = 1, m_F = -1\rangle$, $|F = 1, m_F = 0\rangle$ and $|F = 1, m_F = +1\rangle$, are coupled by a pair of Raman lasers. (c) A schematic diagram about how to use SOC to create spin correlation between the ultracold atoms. Under the strong atom-atom collision interactions, all ultracold atoms are forced to occupy the same many-body quantum state. As a result, the momentum for each atom has the same term. This identical momentum acts as a bus, generating an effective spin-spin interaction.

Orbit-induced spin-spin interaction. For the Hamiltonian (2), it seems that no spin-spin interaction can be found, i.e., spin squeezing cannot be achieved. In fact, we can demonstrate, as shown in Fig. 1(c), that the spin-spin interaction can be induced by the momentum, i.e., $\sim i(a^\dagger - a)$, which reflects the orbital degree of freedom of the ultracold atoms. To prove this argument clearly, we employ a unitary transformation, $U = \exp[iG(a^\dagger + a)S_z]$ with $G = \sqrt{2}\gamma\sqrt{m\hbar\omega_x}/(\hbar\omega_xN)$, to rewrite the Hamiltonian (2) as $H' = \hbar\omega_xNa^\dagger a - \hbar qS_z^2 + \hbar\Omega S_x\cos\left[G\left(a^\dagger + a\right)\right] - \hbar\Omega S_y\sin\left[G\left(a^\dagger + a\right)\right]$, where $q = 4m\gamma^2/(\hbar N) = 8E_L/(\hbar N)$ and E_L is the recoil energy. In experiment of NIST, the trap frequency ω_x and the Rabi frequency Ω are of the orders of 10 Hz and kHz, respectively. For a large atom number, we have $\omega_xN \gg \max\left(\Omega, \sqrt{2}\gamma\sqrt{m\omega_x/\hbar}\right)$ and thus $\langle a^\dagger a\rangle \sim 0$, since $\langle a^\dagger a\rangle$ is inversely proportional to ω_xN[21]. This means that the term $\hbar\Omega S_y\ \sin\ [G(a^\dagger + a)]$ can be omitted safely and $\hbar\Omega S_x\cos\left[G\left(a^\dagger + a\right)\right] \simeq \hbar\Omega S_x$. Finally, we obtain an effective Hamiltonian

$$H' = -\hbar qS_z^2 + \hbar\Omega S_x. \qquad (3)$$

Before proceeding, we check the validity of the Hamiltonian (3) by investigating the ground-state properties, as well as the time-dependent spin dynamics, under current experimental parameters of NIST[7]. As shown in the Methods section, the atom population for the Hamiltonian (3) is derived by $|\langle S_z\rangle| = 0$ for $\gamma^2 \le \hbar\Omega/(4m)$ and $|\langle S_z\rangle|/N = N(4m\gamma^2 + \hbar\Omega)\sqrt{(4m\gamma^2 - \hbar\Omega)}/[8m\gamma^2(4m\gamma^2 + \hbar\Omega)]$ for

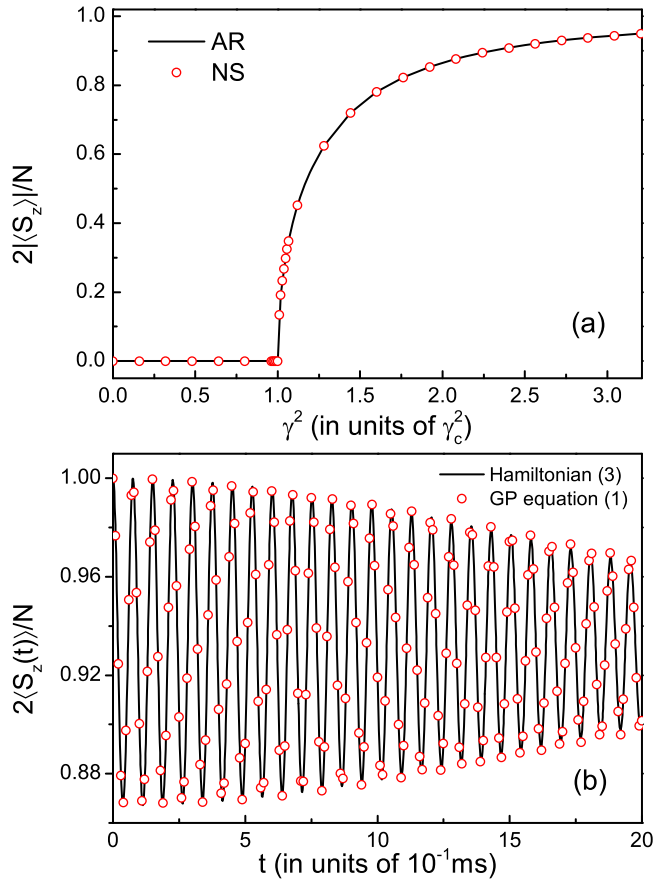

Figure 2 | The ground-state properties and the time-dependent spin dynamics for both the Hamiltonian (3) and the GP equation (1). (a) The atom population $2|\langle S_z\rangle|/N$ as a function of the strength of SOC, when $N = 1.8 \times 10^5$. The critical point is evaluated as $\gamma_c \approx 0.003$ m/s. The black line denotes the analytical result (AR) (see the Methods section), whereas the red open symbol reflects the direct numerical simulation (NS) of the GP equation (1). (b) The time-dependent spin dynamics $2\langle S_z(t)\rangle/N$ for both the Hamiltonian (3) and the GP equation (1), when $N = 2 \times 10^3$. Initially, all ultracold atoms are prepared as the spin-↑ component. Here the black line and the red open symbol denote the numerical results for the Hamiltonian (3) and the GP equation (1), respectively. In (a) and (b), the other parameters are chosen as the experimental parameters, i.e., $m = 1.44 \times 10^{-25}$ kg, $\lambda = 804.1$ nm, $\omega_x = 2\pi \times 50$ Hz, and $\Omega = 2\pi \times 17.8$ kHz.

$\gamma^2 > \hbar\Omega/(4m)$. This analytical result agrees well with the direct numerical simulation of the GP equation (1), as shown in Fig. 2(a), as well as the experimental observation[31]. In addition, the spin dynamics for the Hamiltonian (3) is also similar to that of the GP equation (1), as shown in Fig. 2(b). Based on the above demonstrations, we can argue that the spin properties for the trapped BEC, with the equal Rashba and Dresselhaus SOCs, can be described by the generalized one-axis twisting model (3).

The Hamiltonian (3) is a key result of this report. It shows clearly that the effective spin-spin interaction is generated by controlling the orbital degree of freedom (i.e., the momentum) of the ultracold atoms. If the realized SOC disappears ($\gamma = 0$), the Hamiltonian (3) reduces to the form $H' = \hbar\Omega S_x$, in which no spin-spin interaction can be found. In fact, the spin-spin interaction can also be realized by controlling the direct atom-atom collision interactions via Feshbach resonance. However, its strength $\nu(= (g_{\uparrow\uparrow} + g_{\downarrow\downarrow} - 2g_{\uparrow\downarrow})/4)$ is still very weak in current experimental setups. For example, in the experiment of producing spin squeezing[46], the spin-spin interaction strength $\nu = 2\pi \times 0.063$ Hz, when $N = 2300$. Moreover, this direct spin-spin interaction usually induces atom decoherence and dissipations, which limit the achievable squeezing factor[52,53]. In addition, in atom-cavity interacting systems, the virtual photon can also generate a weak spin-spin interaction[56,57]. Compared with the previous results, our proposal in this report has two advantages. The first is that the generated interaction induced by the orbit is an indirect spin-spin interaction, which does not lead to the atom decoherence and dissipations. The other is that the corresponding spin-spin interaction strength can reach a large value. For instance, when we choose $N = 2300$ in the experimental setup of NIST, $q = 2\pi \times 6.175$ Hz, which has 2 orders larger than ν. This strong spin-spin interaction will generate a giant spin squeezing factor.

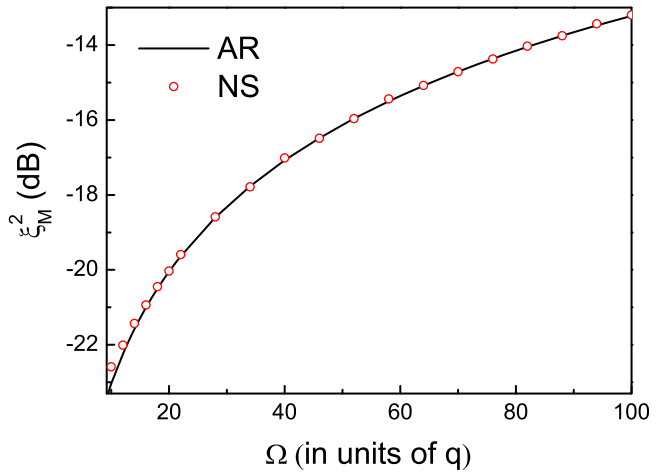

Figure 3 | The maximal squeezing factor ξ_M^2 as a function of the Rabi frequency Ω. The black solid line stands for the analytical result (AR) in Eq. (5), whereas the red open symbol reflects the direct numerical simulation (NS). The atom number is chosen as $N = 2 \times 10^3$.

Spin squeezing. In the absence of the Rabi frequency ($\Omega = 0$), the Hamiltonian (3) reduces to the form $H = -\hbar q S_z^2$, in which the squeezing factor was demonstrated analytically to scale as $N^{-2/3}$ [37]. However, in our proposal, the Rabi frequency Ω cannot be considered to be zero. In fact, it ranges from 10^{-2} kHz to MHz, and thus satisfies the condition of $\Omega \gg q$ in current experimental setup[7]. In such a case, the squeezing factor can be derived from the frozen-spin approximation[40].

We first consider the following initial coherent spin state $|\psi_0\rangle = (|\uparrow\rangle + |\downarrow\rangle)^{\otimes N}/2^{N/2}$, with the mean spin $\langle S_x(0)\rangle = N/2$ and $\langle S_y(0)\rangle = \langle S_z(0)\rangle = 0$. For a weak spin-spin interaction q (or strong Rabi frequency Ω) in the Hamiltonian (3), all ultracold atoms are almost uncorrected in the framework of this prepared coherent spin state. As a result, the quantum noise is evenly distributed in the yz components of spin, namely, $\Delta S_y^2(0) = \Delta S_z^2(0) = N/4$, which is governed by the standard Heisenberg uncertainty relation $\Delta S_y(0)\Delta S_z(0) = |\langle S_x(0)\rangle|/2$, where $\Delta A^2 = \langle A^2\rangle - \langle A\rangle^2$ is the standard deviation. This quantum noise leads to the standard quantum limit, if the coherent spin state is used in a Ramsey interferometer, such as an atom clock[38]. In order to reduce variance of one spin quadrature in the yz plane (the variance of the orthogonal one increases), quantum correlation between the ultracold atoms is very important, and results in a spin-squeezing state[37]. For the given initial coherent spin state in the Hamiltonian (3), quantum correlation can be created by increasing the nonlinear spin-spin interaction (or decreasing the Rabi frequency). Moreover, the corresponding squeezing factor is defined as[40]

$$\xi_z^2(t) = \frac{4\Delta S_z^2(t)}{N}, \tag{4}$$

where $\Delta S_z^2(t) = \langle S_z^2(t)\rangle - \langle S_z(t)\rangle^2$. Since $\langle S_z(t)\rangle$ stands for the atom population, Eq. (4) is also called the atom squeezing factor. If $\xi_z^2 < 1$, all ultracold atoms are squeezed, and vice versa.

We now obtain the explicit solution of Eq. (4) by applying the Heisenberg equation of motion, with respect to the collective spin operators S_y and S_z in the Hamiltonian (3), namely, $\dot{S}_z = \Omega S_y$ and $\dot{S}_y = -\Omega S_z - q(S_z S_x + S_x S_z)$. In general, these differential equations cannot be solved analytically. However, when $\Omega \gg q$, $2\langle S_x(t)\rangle/N$ remains approximately unchanged under the initial state $|\psi_0\rangle$. This implies that we can make an approximation by replacing S_x by $N/2$, which leads to the following harmonic solutions: $S_z(t) \simeq S_z(0)\cos(\omega t) + \Omega S_y(0)\sin(\omega t)/\omega$ and $S_y(t) \simeq -\omega S_z(0)\sin(\omega t)/\Omega + S_y(0)\cos(\omega t)$, where $\omega = \sqrt{\Omega^2 + Nq\Omega}$. Based on these solutions, we have $\Delta S_z^2(t) = N\left[\cos^2(\omega t) + \Omega^2\sin^2(\omega t)/\omega^2\right]/4$ and $\Delta S_y^2(t) = N\left[\cos^2(\omega t) + \omega^2\sin^2(\omega t)/\Omega^2\right]/4$. Since $\omega > \Omega$, the reduced spin fluctuations occurs in the z direction. Moreover, when $t = (2n+1)\pi/(2\omega)$ with $n = 0,1,2,\cdots$, the maximal squeezing factor is obtained by

$$\xi_M^2 = \frac{\Omega^2}{\omega^2} = \frac{1}{1 + qN/\Omega}, \tag{5}$$

In Fig. 3, we compare the analytical result in Eq. (5) with the direct numerical simulation. When $\Omega \gg q$, the analytical result agrees well with the numerical calculation. It implies that the orbit-induced spin squeezing can be well described by the formula (5) in the case of $\Omega \gg q$. Based on Eq. (5), we find that if we choose current experimental parameters, especially with $\Omega = 50q$ and $N = 1.8 \times 10^5$ [7], the maximal squeezing factor can reach $\xi_M^2 = -35.6$ dB. This giant squeezing factor is far larger than previous ones[51]. In Fig. 4, we numerically plot the maximal squeezing factor as a function of the phase ϕ of the initial state, defined as $|\psi_\phi\rangle = (|\uparrow\rangle + e^{i\phi}|\downarrow\rangle)^{\otimes N}/2^{N/2}$. This figure shows that the maximal squeezing factor depends strongly on the phase ϕ. It means that if we choose a proper phase ϕ in preparing the initial state, the maximal squeezing factor can also be largely enhanced.

Discussion

In summary, we have proposed a new way to generate the spin-spin interaction by controlling the orbital degree of freedom (i.e., the momentum) of the ultracold atoms in the trapped BEC, with the equal Rashba and Dresselhaus SOCs. More importantly, a giant spin squeezing factor (lower than -30 dB) has been achieved by manipulating a pair of Raman lasers. We have also found that the maximal squeezing factor can be largely enhanced by tuning the phase of the prepared initial state. We hope that our predictions could be observed in future experiments, since spin squeezing has an important concept in quantum information, and moreover, are closely related to design the best atomic clocks.

Methods

Ground-state properties under a mean-field method. Here we employ the Holstein-Primakoff transformation and boson expansion method to discuss the ground-state properties of the Hamiltonian (3)[58]. By means of the Holstein-Primakoff transformation, which is defined as $S_+ = c^\dagger\sqrt{N - c^\dagger c}$, $S_- = \sqrt{N - c^\dagger c}\,c$, and $S_z = c^\dagger c - N/2$, with $[c, c^\dagger] = 1$, the Hamiltonian (3) is rewritten as

$$H' = -\hbar q\left(c^\dagger c - \frac{N}{2}\right)^2 + \frac{\hbar\Omega}{2}\left(c^\dagger\sqrt{N - c^\dagger c} + \sqrt{N - c^\dagger c}\,c\right). \tag{6}$$

We now introduce a shifting boson operator $d^\dagger = c^\dagger + \sqrt{N}\beta$, where β is a auxiliary parameter to be determined, to describe the collective excitation of the ultracold atoms. Substituting this shifting boson operator $d^\dagger$ into the Hamiltonian (6) and then using the boson expansion method, we have $H' = NH_0 + N^{1/2}H_1 + \cdots = N$

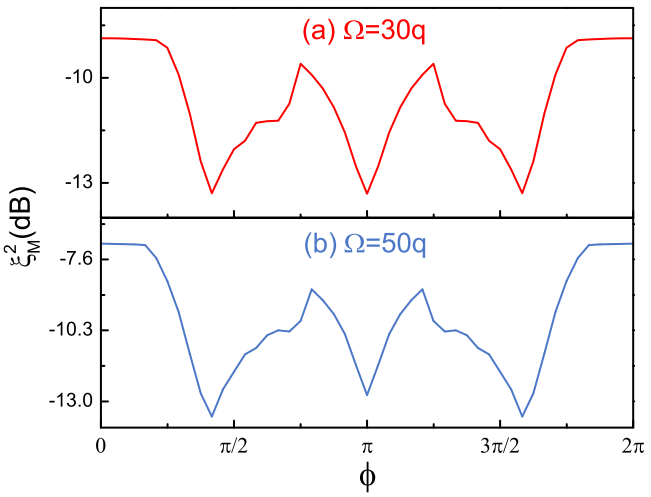

Figure 4 | The maximal squeezing factor ξ_M^2 as a function of the phase ϕ of the prepared initial state. This initial state is defined as $|\psi_\phi\rangle = (|\uparrow\rangle + e^{i\phi}|\downarrow\rangle)^{\otimes N}/2^{N/2}$, with the atom number $N = 200$. The Rabi frequency is chosen as (a) $\Omega = 30q$ and (b) $\Omega = 50q$, respectively.

$\left[\hbar\Omega\beta\sqrt{1-\beta^2} - 4m\gamma^2\left(\beta^2 - \frac{1}{2}\right)^2\right] + N^{1/2}\left[\hbar\Omega(1-2\beta^2)(d^\dagger + d)\Big/\left[2\sqrt{1-\beta^2}\right] - 8m\gamma^2\beta\left(\beta^2 - \frac{1}{2}\right)(d^\dagger + d)\right] + \ldots$.

In terms of the expanded Hamiltonian, the scaled ground-state energy is obtained by[58]

$$\frac{E(\beta)}{N} = \hbar\Omega\beta\sqrt{1-\beta^2} - 4m\gamma^2\left(\beta^2 - \frac{1}{2}\right)^2. \tag{7}$$

The corresponding auxiliary parameter β can be derived from the equilibrium condition $\partial E(\beta)/\partial\beta = 0$. The result is given by

$$\hbar\Omega\eta\left(1+\eta^2\right) - 4m\gamma^2\eta\left(1-\eta^2\right) = 0, \tag{8}$$

where $h\sqrt{1-h^2} = \beta^2 - 1/2\left(1/2 \le h^2 < 1\right)$ and $\eta = h\Big/\sqrt{1-h^2}$. Equation (8) has two solutions, including $\eta = 0$ and $\eta^2 = (4m\gamma^2 - \hbar\Omega)/(4m\gamma^2 + \hbar\Omega)$. Finally, with the help of the stability condition $\partial^2 E(\beta)/\partial\beta^2 > 0$, we obtain $\eta = 0$ for $\gamma^2 \le \hbar\Omega/(4m)$ and $\sqrt{(4m\gamma^2 - \hbar\Omega)/(4m\gamma^2 + \hbar\Omega)}$ for $\gamma^2 > \hbar\Omega/(4m)$. This implies that the Hamiltonian (3) exhibits a quantum phase transition from a zero-momentum phase ($\eta = 0$) to a separate phase ($\eta = \sqrt{(4m\gamma^2 - \hbar\Omega)/(4m\gamma^2 + \hbar\Omega)}$) at the critical point $\gamma_c = \sqrt{\hbar\Omega/(4m)}$[21,24,31]. In addition, by means of Eq. (8), the atom population is obtained by

$$|\langle S_z\rangle| = \frac{N\eta}{1+\eta^2} = \begin{cases} 0, & \left(\gamma^2 \le \frac{\hbar\Omega}{4m}\right) \\ \frac{N}{2}\sqrt{\frac{4m\gamma^2 - \hbar\Omega}{4m\gamma^2 + \hbar\Omega}}\frac{4m\gamma^2 + \hbar\Omega}{4m\gamma^2}, & \left(\gamma^2 > \frac{\hbar\Omega}{4m}\right) \end{cases}. \tag{9}$$

1. Nagaosa, N., Sinova, J., Onoda, S., MacDonald, A. H. & Ong, N. P. Anomalous Hall effect. *Rev. Mod. Phys.* **82**, 1539–1592 (2010).
2. Xiao, D., Chang, M.-C. & Niu, Q. Berry phase effects on electronic properties. *Rev. Mod. Phys.* **82**, 1959–2007 (2010).
3. Qi, X.-L. & Zhang, S.-C. Topological insulators and superconductors. *Rev. Mod. Phys.* **83**, 1057–1110 (2011).
4. Žutić, I., Fabian, J. & Das Sarma, S. Spintronics: fundamentals and applications. *Rev. Mod. Phys.* **76**, 323–410 (2004).
5. Nayak, C., Simon, S. H., Stern, A., Freedman, M. & Das Sarma, S. Non-Abelian anyons and topological quantum computation. *Rev. Mod. Phys.* **80**, 1083–1159 (2008).
6. Stanescu, T. D., Anderson, B. & Galitski, V. Spin-orbit coupled Bose-Einstein condensates. *Phys. Rev. A* **78**, 023616 (2008).
7. Lin, Y.-J., Jimenez-Garcia, K. & Spielman, I. B. Spin-orbit-coupled Bose-Einstein condensates. *Nature* **471**, 83–86 (2011).
8. Larson, J. & Sjöqvist, E. Jahn-Teller-induced Berry phase in spin-orbit-coupled Bose-Einstein condensates. *Phys. Rev. A* **79**, 043627 (2009).

9. Wang, C., Gao, C., Jian, C.-M. & Zhai, H. Spin-orbit coupled spinor Bose-Einstein condensates. *Phys. Rev. Lett.* **105**, 160403 (2010).
10. Ho, T.-L. & Zhang, S. Bose-Einstein condensates with spin-orbit interaction. *Phys. Rev. Lett.* **107**, 150403 (2011).
11. Sinha, S., Nath, R. & Santos, L. Trapped two-dimensional condensates with synthetic spin-orbit coupling. *Phys. Rev. Lett.* **107**, 270401 (2011).
12. Xu, X.-Q. & Han, J. H. Spin-orbit coupled Bose-Einstein condensate under rotation. *Phys. Rev. Lett.* **107**, 200401 (2011).
13. Xu, X.-Q. & Han, J. H. Emergence of chiral magnetism in spinor Bose-Einstein condensates with Rashba coupling. *Phys. Rev. Lett.* **108**, 185301 (2012).
14. Wu, C.-J., Mondragon-Shem, I. & Zhou, X.-F. Unconventional Bose-Einstein condensations from spin-orbit coupling. *Chin. Phys. Lett.* **28**, 097102 (2011).
15. Yip, S.-K. Bose-Einstein condensation in the presence of artificial spin-orbit interaction. *Phys. Rev. A* **83**, 043616 (2011).
16. Xu, Z. F., Lü, R. & You, L. Emergent patterns in a spin-orbit-coupled spin-2 Bose-Einstein condensate. *Phys. Rev. A* **83**, 053602 (2011).
17. Zhou, X.-F., Zhou, J. & Wu, C. Vortex structures of rotating spin-orbit-coupled Bose-Einstein condensates. *Phys. Rev. A* **84**, 063624 (2011).
18. Kawakami, T., Mizushima, T. & Machida, K. Textures of $F = 2$ spinor Bose-Einstein condensates with spin-orbit coupling. *Phys. Rev. A* **84**, 011607(R) (2011).
19. Fu, Z., Wang, P., Chai, S., Huang, L. & Zhang, J. Bose-Einstein condensate in a light-induced vector gauge potential using 1064-nm optical-dipole-trap lasers. *Phys. Rev. A* **84**, 043609 (2011).
20. Zhu, Q., Zhang, C. & Wu, B. Exotic superfluidity in spin-orbit coupled Bose-Einstein condensates. *EPL* **100**, 50003 (2012).
21. Zhang, Y., Chen, G. & Zhang, C. Tunable spin-orbit coupling and quantum phase transition in a trapped Bose-Einstein condensate. *Sci. Rep.* **3**, 1937 (2013).
22. Zhang, Y., Mao, L. & Zhang, C. Mean-field dynamics of spin-orbit coupled Bose-Einstein condensates. *Phys. Rev. Lett.* **108**, 035302 (2012).
23. Hu, H., Ramachandhran, B., Pu, H. & Liu, X.-J. Spin-orbit coupled weakly interacting Bose-Einstein condensates in harmonic traps. *Phys. Rev. Lett.* **108**, 010402 (2012).
24. Li, Y., Pitaevskii, L. P. & Stringari, S. Quantum tricriticality and phase transitions in spin-orbit coupled Bose-Einstein condensates. *Phys. Rev. Lett.* **108**, 225301 (2012).
25. Lian, J. *et al.* Thermodynamics of spin-orbit-coupled Bose-Einstein condensates. *Phys. Rev. A* **86**, 063620 (2012).
26. Ozawa, T. & Baym, G. Stability of ultracold atomic Bose condensates with Rashba spin-orbit coupling against quantum and thermal fluctuations. *Phys. Rev. Lett.* **109**, 025301 (2012).
27. Ozawa, T. & Baym, G. Ground-state phases of ultracold bosons with Rashba-Dresselhaus spin-orbit coupling. *Phys. Rev. A* **85**, 013612 (2012).
28. Kawakami, T., Mizushima, T., Nitta, M. & Machida, K. Stable skyrmions in *SU*(2) gauged Bose-Einstein condensates. *Phys. Rev. Lett.* **109**, 015301 (2012).
29. Radić, J., Ciolo, A. D., Sun, K. & Galitski, V. Exotic quantum spin models in spin-orbit-coupled Mott insulators. *Phys. Rev. Lett.* **109**, 085303 (2012).
30. Cole, W. S., Zhang, S., Paramekanti, A. & Trivedi, N. Bose-Hubbard models with synthetic spin-orbit coupling: Mott insulators, spin textures, and superfluidity. *Phys. Rev. Lett.* **109**, 085302 (2012).
31. Zhang, J.-Y. *et al.* Collective dipole oscillations of a spin-orbit coupled Bose-Einstein condensate. *Phys. Rev. Lett.* **109**, 115301 (2012).
32. Zhang, D.-W., Xue, Z.-Y., Yan, H., Wang, Z. D. & Zhu, S.-L. Macroscopic Klein tunneling in spin-orbit-coupled Bose-Einstein condensates. *Phys. Rev. A* **85**, 013628 (2012).
33. Zhang, D.-W., Fu, L.-B., Wang, Z. D. & Zhu, S.-L. Josephson dynamics of a spin-orbit-coupled Bose-Einstein condensate in a double-well potential. *Phys. Rev. A* **85**, 043609 (2012).
34. Xu, Z. F., Kawaguchi, Y., You, L. & Ueda, M. Symmetry classification of spin-orbit-coupled spinor Bose-Einstein condensates. *Phys. Rev. A* **86**, 033628 (2012).
35. Chen, G., Ma, J. & Jia, S. Long-range superfluid order in trapped Bose-Einstein condensates with spin-orbit coupling. *Phys. Rev. A* **86**, 045601 (2012).
36. Zhang, Y. & Zhang, C. BEC in spin-orbit coupled optical lattices: flat bands and superfluidity. *Phys. Rev. A* **87**, 023611 (2013).
37. Kitagawa, M. & Ueda, M. Squeezed spin states. *Phys. Rev. A* **47**, 5138–5143 (1993).
38. Santarelli, G. *et al.* Quantum projection noise in an atomic fountain: a high stability Cesium frequency standard. *Phys. Rev. Lett.* **82**, 4619–4622 (1999).
39. Sørensen, A., Duan, L.-M., Cirac, J. I. & Zoller, P. Many-particle entanglement with Bose-Einstein condensates. *Nature* **409**, 63–66 (2001).
40. Ma, J., Wang, X., Sun, C. P. & Nori, F. Quantum spin squeezing. *Phys. Rep.* **509**, 89–165 (2011).
41. Helmerson, K. & You, L. Creating massive entanglement of Bose-Einstein condensed atoms. *Phys. Rev. Lett.* **87**, 170402 (2001).
42. Zhang, M., Helmerson, K. & You, L. Entanglement and spin squeezing of Bose-Einstein-condensed atoms. *Phys. Rev. A* **68**, 043622 (2003).
43. Ng, H. T., Law, C. K. & Leung, P. T. Quantum-correlated double-well tunneling of two-component Bose-Einstein condensates. *Phys. Rev. A* **68**, 013604 (2003).
44. Jin, G.-R. & Kim, S. W. Storage of spin squeezing in a two-component Bose-Einstein condensate. *Phys. Rev. Lett.* **99**, 170405 (2007).
45. Estève, J., Gross, C., Weller, A., Giovanazzi, S. & Oberthaler, M. K. Squeezing and entanglement in a Bose-Einstein condensate. *Nature* **455**, 1216–1219 (2008).
46. Gross, C., Zibold, T., Nicklas, E., Estève, J. & Oberthaler, M. K. Nonlinear atom interferometer surpasses classical precision limit. *Nature* **464**, 1165–1169 (2010).
47. Riedel, M. F. *et al.* Atom-chip-based generation of entanglement for quantum metrology. *Nature* **464**, 1170–1173 (2010).
48. Bookjans, E. M., Hamley, C. D. & Chapman, M. S. Strong quantum spin correlations observed in atomic spin mixing. *Phys. Rev. Lett.* **107**, 210406 (2011).
49. Liu, Y. C., Xu, Z. F., Jin, G. R. & You, L. Spin squeezing: transforming one-axis twisting into two-axis twisting. *Phys. Rev. Lett.* **107**, 013601 (2011).
50. Chin, C., Grimm, R., Julienne, P. & Tiesinga, E. Feshbach resonances in ultracold gases. *Rev. Mod. Phys.* **82**, 1225–1286 (2010).
51. Robins, N. P., Altin, P. A., Debs, J. E. & Close, J. D. Atom lasers: Production, properties and prospects for precision inertial measurement. *Phys. Rep.* **529**, 265–296 (2013).
52. Li, Y., Castin, Y. & Sinatra, A. Optimum spin squeezing in Bose-Einstein condensates with particle losses. *Phys. Rev. Lett.* **100**, 210401 (2008).
53. Bar-Gill, N., Bhaktavatsala Rao, D. D. & Kurizki, G. Creating nonclassical states of Bose-Einstein condensates by dephasing collisions. *Phys. Rev. Lett.* **107**, 010404 (2011).
54. Dicke, R. H. Coherence in spontaneous radiation processes. *Phys. Rev.* **93**, 99–110 (1954).
55. Pu, H. & Bigelow, N. P. Collective excitations, metastability, and nonlinear response of a trapped two-species Bose-Einstein condensate, *Phys. Rev. Lett.* **80**, 1134 (1998).
56. Agarwal, G. S., Puri, R. R. & Singh, R. P. Atomic Schröinger cat states. *Phys. Rev. A* **56**, 2249–2254 (1997).
57. Leroux, I. D., Schleier-Smith, M. H. & Vuletić, V. Implementation of cavity squeezing of a collective atomic spin. *Phys. Rev. Lett.* **104**, 073602 (2010).
58. Emary, C. & Brandes, T. Chaos and the quantum phase transition in the Dicke model. *Phys. Rev. E* **67**, 066203 (2003).

Acknowledgments

We thank Prof. Chuanwei Zhang and Dr. Yongping Zhang for their helpful discussions. This work is supported by the 973 Program under Grant No. 2012CB921603, the NNSFC under Grant Nos. 10934004, 11074154, 11075099, 11275118, and 61275211, the International Science and Technology Cooperation Program of China under Grant No.2001DFA12490, and ZJNSF under Grant No. LY13A040001.

Author contributions

J.L., L.Y., J.-Q.L., G.C. and S.J. conceived the idea, J.L., L.Y. and G.C. performed the calculation, J.-Q.L., G.C. and S.J. wrote the manuscript, G.C. supervised the whole research project.

Additional information

Competing financial interests: The authors declare no competing financial interests.

How to cite this article: Lian, J.L., Yu, L.X., Liang, J.-Q., Chen, G. & Jia, S.T. Orbit-induced spin squeezing in a spin-orbit coupled Bose-Einstein condensate. *Sci. Rep.* **3**, 3166; DOI:10.1038/srep03166 (2013).